Experimental study of the spin density of metastable fcc ferromagnetic Fe-Cu alloys

L. E. Bove, C. Petrillo, and F. Sacchetti
Istituto Nazionale per la Fisica della Materia, Unitá di Perugia, Perugia, Italy
and Dipartimento di Fisica, Universitá di Perugia, Via Alessandro Pascoli, I-06123 Perugia, Italy

G. Mazzone
Ente per le Nuove Tecnologie, l'Energia e l'Ambiente (ENEA), Centro Ricerche Casaccia, Divisione Nuovi Materiali, Roma, Italy
(Received 18 October 1999)

Magnetization density measurements on metastable Fe_xCu_{1-x} alloys at four compositions ($x=20$, 40, 50, and 60 at. %) and at 5 K temperature were carried out by means of polarized neutron diffraction. The samples were produced by high-energy ball milling and characterized by x-ray diffraction and fluorescence measurements. Additional bulk magnetization measurements were carried out on the two samples at high Fe concentration. Over the present concentration region, the Fe-Cu system is ferromagnetic and the four samples were found to be in the fcc phase. Fe-Cu is therefore a very suitable system to investigate the magnetic state of Fe in an fcc environment. Other than confirming that the Fe-Cu system is not a simple dilution alloy, the present results were compatible with a two-state model for fcc Fe—that is, two different coexisting electronic states associated with different magnetic moments and form factors.

I. INTRODUCTION

One of the most severe tests for first-principles solid-state theory is the description of the magnetic state of transition metals among which Fe and Mn represent quite difficult cases since their behavior is the result of a fine balance between competing exchange-correlation interactions. In order to perform meaningful tests, it is very important to compare experiment and theory at the same level of accuracy; therefore, the experimental study of the spin density is of particular interest since it can be compared with the results obtained using the local spin density approximation (LSDA), as the spin density is one of the observables which can be derived directly from the theory without additional approximations.[1,2]

Fe has been the subject of several detailed theoretical investigations[3–5] since it can be found in at least four electronic states lying within a very narrow energy range. In fact, although the experimental ground state of Fe at room temperature and standard pressure is the bcc ferromagnetic phase, the energies of the fcc ferromagnetic, antiferromagnetic, and nonmagnetic phases (and even more complex magnetic phases[6]) are very close to that of the ground state. This behavior is in qualitative agreement with the observation that concentrated alloys of Fe with other transition metals are found in all of the above magnetic and crystallographic phases. However, in the equilibrium state, all binary $3d$ metal-iron alloys in the fcc phase contain a second component which is intrinsically magnetic. Typical examples are the fcc systems Fe-Mn,[7,8] Fe-Co,[9] and Fe-Ni.[10–13] Although the experimental investigation of these systems is useful for an understanding of the magnetic behavior of Fe in the fcc lattice, the second component, even at relatively low concentration, may play a decisive role in the choice of the magnetic phase of the system. This point is made clear by a comparison of the behavior of $Fe_{65}Mn_{35}$ (Ref. 8) with $Fe_{66}Ni_{34}$.[13] Even though the lattice parameter of $Fe_{65}Mn_{35}$ is larger than that of $Fe_{66}Ni_{34}$, thus favoring the formation of the high-moment, high-volume ferromagnetic state of Fe,[5] the magnetic moment on the iron atom is lower in $Fe_{65}Mn_{35}$ than in $Fe_{66}Ni_{34}$. Moreover, $Fe_{65}Mn_{35}$ is antiferromagnetic, while $Fe_{66}Ni_{34}$ is ferromagnetic, in contrast with the behavior deduced from LSDA calculations in the case of pure fcc Fe,[5] whose equilibrium magnetic state becomes ferromagnetic as the lattice parameter increases progressively. On the other hand, the overall behavior of fcc Fe-Ni alloys,[10–13] as described by the curve of the bulk magnetization versus composition, shows that competing ferromagnetic-antiferromagnetic interactions are present in fcc Fe. The presence of competing interactions in fcc Fe and Fe-based alloys is affected by the frustrated nature of the collinear antiferromagnetic structure of fcc systems and should be carefully taken into account in all theoretical calculations.[14] Moreover, the competition between ferromagnetic and antiferromagnetic interactions is usually assumed to be the cause of the Invar behavior of fcc Fe-Ni alloys at Ni concentrations close to 35%. Upon heating, in fact, the thermal volume expansion is contrasted by the opposite tendency to volume contraction brought about by the increased fraction of (low-volume) antiferromagnetically aligned atoms.

Considering that pure fcc Fe is stable only at high temperature, where no spontaneous magnetic ordering is observed, some experimental information about its magnetic properties can be obtained by studying fcc Fe-based alloys. However, focusing on fcc Fe requires the contribution from the second component of the alloy to be negligible, so that those alloys where Fe is the only magnetic atom should be preferentially considered. In this respect, Fe-Cu alloys are very well suited to this purpose since metallic Cu, which has a full $3d$ band, is not expected to contribute to the magnetic moment of the system. This is, for instance, the case of Ni-Cu alloys, where a very simple behavior is observed in the trend of the bulk magnetic moment as a function of the alloy composition.[15–18] Ni-Cu alloys have been investigated

widely and now they represent a reference system. Fe-Cu alloys are also very interesting, as the number of the outer electrons ranges from 11 in pure copper to 8 in pure iron, which is a very wide range of $3d$ electron concentration. However, Fe-Cu alloys are only stable as terminal solid solutions in a restricted range of composition close to the pure metals. As a consequence, these alloys can only be studied as metastable phases obtained by nonequilibrium processing techniques.

The high-energy ball milling technique has been shown to be very effective in producing fcc Fe-Cu alloys in the Fe concentration range from 0 to at least 60 at.%.[19] These alloys have been investigated in detail by means of x-ray diffraction, differential calorimetry, and Mössbauer spectroscopy.[19–22] In addition, bulk magnetization measurements[20–22] are also available. The results of these studies have shown that the samples prepared by ball milling are in the fcc phase and extended x-ray absorption fine-structure (EXAFS) measurements have proved that the fcc phase of the alloy is present at the atomic level.[23] Surprisingly, bulk magnetization measurements have been interpreted as providing evidence for a simply diluted ferromagnet with the same magnetic moment of $2.2\mu_B$ per iron atom, as in pure *bcc* Fe. This unexpected conclusion has been criticized on the basis of the known behavior of Fe in the fcc lattice in Ref. 24 where the effect of thermal annealing on the bulk magnetic moment was also discussed. Actually, in the fcc phase, Fe can sustain two possible states of stable magnetic moment—namely, a high-moment ferromagnetic state, corresponding to $(2.7-3)\mu_B$ per iron atom, and a full $3d$ spin-up band[5,11] and a low-moment state, corresponding to $\sim 0.7\mu_B$ per iron atom, characteristic of the antiferromagnetic state.[5,8,9] Therefore, considering that the state of fcc Fe with $2.2\mu_B$/atom has neither been observed in other companion systems nor obtained in first-principles calculations,[3–5] investigation of the magnetic moment distribution of this alloy at the atomic level is extremely important.

In the present study, measurements of the magnetization density of metastable fcc Fe-Cu alloys at different compositions have been carried out by means of polarized neutron diffraction, aiming at describing the magnetic state of Fe in this high-volume fcc environment. Polarized neutrons are particularly suited to this purpose because they couple to the electron spin density and are sensitive to the local structure, so that the effect of the local environment on the magnetic state can be investigated by studying the alloy system at different concentrations.

II. EXPERIMENT

The present samples were obtained by mixing commercially pure Fe (99.95%) and Cu (99.8%) powders at the compositions 20, 40, 50, and 60 Fe at.%. In order to prevent sample oxidation, the starting powders were flushed in Ar for 30 min and then sealed in a container under the same atmosphere. Powder charges of about 5 g were milled for 40 h in steps of 30 min alternated with rest intervals of 5 min, using a SPEX 8000 mixer/mill equipped with a hardened steel vial and two balls of the same material of 13.5 mm diameter and 10 g weight each.

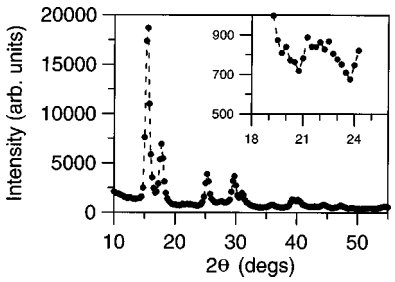

FIG. 1. X-ray diffraction spectrum of $Fe_{60}Cu_{40}$. The typical fcc pattern is observed. The (200) reflection from a bcc-like phase is shown on an expanded scale in the inset.

The microscopic structure of the samples was investigated by means of x-ray diffraction using Ag $K\alpha$ incoming radiation, which allows transmission geometry measurements of relatively thick samples (50 μm). All the samples were found to be in the fcc phase with the residual bcc-like phase always less than 3%. A typical x-ray diffraction spectrum is shown in Fig. 1. Further characterization was carried out by means of x-ray fluorescence, excited using monochromatic Ag $K\alpha$ radiation. No element with an atomic number greater than $Z=14$, other than Fe and Cu, was detected within the sensitivity limits of the experimental apparatus (0.5%). The composition of all the samples was found to be equal to the nominal one. Of course, such an analysis did not allow the actual composition of the fcc Fe-Cu phase to be determined since, as mentioned above, a small fraction of bcc Fe was present. The present samples were found to be very similar to those investigated by other authors,[19,20] as is apparent on comparing the results of the characterization measurements.

Polarized neutron diffraction measurements were performed on the D3 polarized neutron diffractometer installed at the Institut Laue Langevin (Grenoble, France). The instrument was equipped with a superconducting magnet and a cryostat. Use of D3 as a powder diffractometer in this specific experiment demanded for an improvement in resolution, achievable by selecting the highest possible take-off angle at the monochromator. The (200) Bragg reflection from a $Co_{92}Fe_8$ monochromator was, therefore, selected to produce the polarized neutron beam with 0.843 Å wavelength. With this configuration, a resolution adequate for a good separation of the (111) and (200) reflections in the present samples was attained and a rather extended $\sin(\vartheta)/\lambda$ region was accessible. The chosen monochromator configuration also limited the half-wavelength contamination, which was further reduced by means of an Er filter.

The powder samples were contained in a cylinder-shaped vanadium cell of 8 mm internal diameter, 0.5 mm wall thickness, and 20 mm height. Because of the very irregular distribution of particle size in the present samples, the highest available magnetic field, namely, 4.6 T, was used in every measurement. A test performed on the flipping ratio of the $Fe_{50}Cu_{50}$ sample at 5 K showed that such a field was adequate to get full magnetic saturation. Indeed, from bulk magnetization measurements[20,21] it is known that the saturation field is much lower than the present one, which, however, was necessary to reduce the depolarization of the neutron beam. The measurements were carried out at 5 K. Data were collected over the 2ϑ scattering angle range from 15° to 80° in steps of 0.5°, resulting in a $\sin(\vartheta)/\lambda$ range from

TABLE I. Expected, R^{th}, and measured, R^{expt}, flipping ratios of the polarization analyzer $Co_{92}Fe_8$ (see text). The experimental data were collected on Fe-Cu samples at 5 K. The experimental values of the spin reversal probability w, due to sample depolarization, are listed in the last column (see the Appendix).

	R^{th}	R^{expt}	w
$Fe_{20}Cu_{80}$	34.0	34.0±1.0	0.000±0.005
$Fe_{40}Cu_{60}$	34.0	28.3±0.7	0.014±0.005
$Fe_{50}Cu_{50}$	34.0	14.9±0.5	0.091±0.005
$Fe_{60}Cu_{40}$	34.0	7.9±0.2	0.224±0.005

0.15 to 0.77 $Å^{-1}$. Consequently, the highest-order reflections measured in the present experiment were (511) and (333). The background intensity, which represents quite a large contribution to the scattered intensity because of the various thermal shieldings inside the cryostat, was also measured at 5 K. Two background scans were performed, one with the empty container and one with the container filled with B_4C powder as a full absorber. Using these results, the background expected in presence of the sample, taking into account the sample transmission (which was in the range 0.6–0.7), could be deduced.

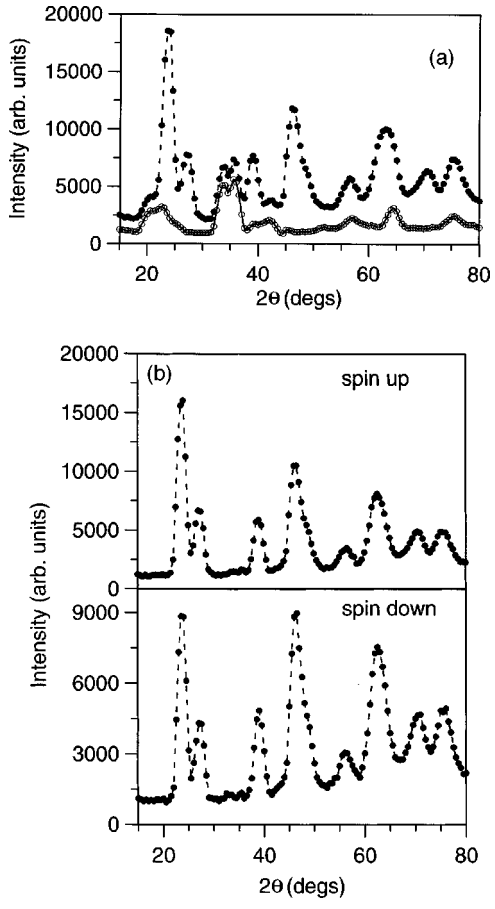

FIG. 2. (a) Diffracted intensity from $Fe_{60}Cu_{40}$ at 5 K for spin-up incoming neutrons vs scattering angle (dots). The background intensity I_{back} [see Eq. (A1)] for spin-up incoming neutrons at the same temperature is also shown (circles). Lines are a guide to the eye. (b) Background-free intensity vs scattering angle in $Fe_{60}Cu_{40}$ at 5 K. Upper panel, spin up; lower panel, spin down.

Depolarization effects were measured by inserting a thin single crystal of $Co_{92}Fe_8$ inside the powder sample and at the center of the cell. The size of the $Co_{92}Fe_8$ crystal, $0.3\times6\times22\,mm^3$, was such that the depolarization effects could be measured as an average on the whole beam section. The same experimental configuration as for the diffraction measurements was used. By measuring the flipping ratio of the (200) reflection of the $Co_{92}Fe_8$ sample and from the known theoretical values of the flipping ratio as a function of neutron polarization, the probability of depolarization of the neutron beam in crossing the first half of the sample was obtained. The measurement was repeated for all the samples because the particle size depended on sample composition. The effect caused by the depolarization is apparent from Table I where the measured and expected flipping ratio values of $Co_{92}Fe_8$ are reported at 5 K for the various samples. The depolarization is quite appreciable for the samples with the highest iron content, which, in turn, are those whose particle size is smaller.

The diffraction data on the Fe-Cu alloys were analyzed according to the procedure described in the Appendix, which basically consists of background substraction, correction for incomplete beam polarization, depolarization effects, and spin-dependent attenuation. As an example, the intensity measured with spin-up incoming neutrons on the sample $Fe_{60}Cu_{40}$ at 5 K is shown in Fig. 2(a) in comparison with the background intensity at the same temperature. The background-free intensities for the $Fe_{60}Cu_{40}$ sample at 5 K are shown in Fig. 2(b) for spin-up and spin-down incoming neutrons. From the corrected spin-up and spin-down data, the integrated intensities and the flipping ratios were obtained for each Bragg reflection. Finally, from the ratios of magnetic to nuclear scattering amplitudes, the magnetic structure factors $F_M(\mathbf{G})$ of the present samples at 5 K were deduced. The magnetic structure factors $F_M(\mathbf{G})$ are reported in Table II, and the quoted errors account for both the statistical errors and uncertainties affecting the applied corrections.

TABLE II. Magnetic structure factors $F_M(\mathbf{G})$ (μ_B/atom) as obtained from the present measurements at 5 K. The entries at the (000) reflection are the bulk magnetic moments as reported in Ref. 20 for the 20 and 40 at.% alloys and as obtained from present measurements for the 50 and 60 at.% alloys.

	$T=5$ K			
(hkl)	$Fe_{20}Cu_{80}$ (μ_B/atom)	$Fe_{40}Cu_{60}$ (μ_B/atom)	$Fe_{50}Cu_{50}$ (μ_B/atom)	$Fe_{60}Cu_{40}$ (μ_B/atom)
0 0 0	0.439±0.002	0.920±0.002	1.055±0.002	1.086±0.002
1 1 1	0.239±0.009	0.564±0.009	0.651±0.007	0.666±0.010
2 0 0	0.215±0.018	0.498±0.016	0.606±0.013	0.588±0.023
2 2 0	0.108±0.012	0.243±0.012	0.281±0.007	0.296±0.016
3 1 1	0.075±0.006	0.100±0.019	0.236±0.007	0.224±0.007
2 2 2	0.078±0.021	0.140±0.025	0.197±0.016	0.198±0.016
4 0 0	0.051±0.021	0.131±0.028	0.137±0.016	0.159±0.026
3 3 1	0.015±0.012	0.072±0.006	0.060±0.010	0.078±0.016
4 2 0	0.027±0.012	0.041±0.009	0.064±0.013	0.117±0.020
4 2 2	0.009±0.015	0.034±0.012	0.067±0.016	0.055±0.020
5 1 1	−0.021±0.015	0.037±0.012	0.038±0.016	0.007±0.017
3 3 3				

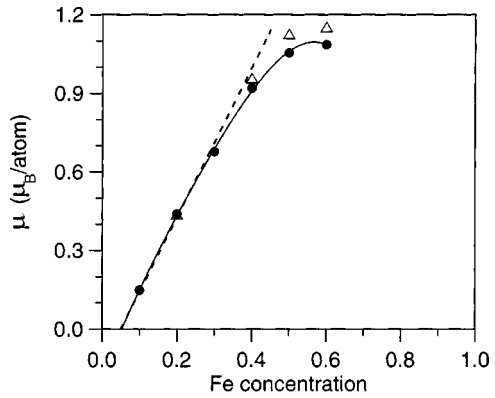

FIG. 3. Magnetic moment per atom vs Fe concentration in Fe-Cu alloys. Dots: bulk magnetization data (μ). Open triangles: polarized neutron diffraction data ($\mu_{\rm fit}$). The solid line is a guide to the eye. The dashed curve is the line with $2.85\mu_B$/atom slope through 0.05 Fe concentration.

Finally, bulk magnetization measurements were carried out on the 50 and 60 at. % alloys using the same samples and at the same temperature (5 K) and applied magnetic field (4.6 T) as the neutron experiment. The reasons for repeating the magnetization measurements at these Fe concentrations were suggested by some discrepancies between the values reported in the literature.[20,21] The bulk magnetization data are also quoted in Table II as the structure factors of the (000) reflection, and the values at 20 and 40 at.% concentrations are after Refs. 20 and 21.

III. DATA ANALYSIS AND DISCUSSION

By means of the combined use of the present neutron diffraction and bulk magnetization data at four Fe concentrations, information on the microscopic arrangement of the magnetic moment in the Fe-Cu system and, ultimately, on the magnetic state of Fe in an fcc environment is gained. The analysis of the neutron diffraction data and their interpretation are strictly related to the knowledge of the bulk magnetization curve versus composition. The bulk magnetic moment data are shown in Fig. 3. Some observations on the behavior of the Fe-Cu system can be drawn immediately from an inspection of this figure. The region of linear dependence at low Fe concentrations is followed by a nonlinear dependence region for Fe concentrations higher than 30%. Moreover, from the trend of the bulk magnetization curve at low Fe concentrations, it is clear that no spontaneous magnetization occurs when the Fe concentration is less than $\sim$5 at. %. Although this feature was not explicitly stated in previous papers, it is quite apparent in all the reported experimental bulk magnetization data and Curie temperature, even though the exact onset concentration is not accurately defined.[20,25,26] Increasing the Fe concentration, the onset of spontaneous magnetization is observed and the system behaves as a ferromagnet. In the Fe concentration region from 5% up to 30%, the magnetic moment per atom increases at a rate of about $2.85\mu_B$/atom; that is, each iron atom added to the alloy introduces an additional magnetic moment of $2.85\mu_B$. This concentration derivative of the average magnetic moment is related to the neutron diffuse scattering cross section.[16,18] In the present case, the relatively high value of the derivative can be taken as an indication that Cu atoms do not carry a magnetic moment. This is also supported by the results obtained in the Ni-Cu alloys, where a qualitatively similar behavior was observed and polarized diffuse neutron scattering data were available.[16,18] In Fig. 3, a straight line with $2.85\mu_B$/atom slope and intercepting the concentration axis at $x_{\rm Fe}=0.05$ is also shown. Even from this initial observation, it is evident that the Fe-Cu system *cannot be described as simple dilution of Fe into Cu*, contrary to what was stated in Ref. 20.

The behavior of the bulk magnetization curve at Fe concentration lower than $\sim$30% can be described by a simple phenomenological model which accounts for both the linear trend and the onset concentration for ferromagnetism and offers a possible interpretation of the physical mechanism leading to the observed magnetic behavior. The electronic structure of the binary $3d$ alloy can be described, as usual, by means of two different electronic bands associated with each component of the alloy and each one comprising two spin-dependent subbands. In a system like Fe-Cu, where the second component is nonmagnetic, the polarization of the Cu bands, as also discussed above, can be reasonably neglected as a first approximation. A further assumption can be done on the $3d$ band of Fe which, in this alloy, is in an fcc environment: the spin-up $3d$ band of Fe can be taken as full at all the alloy concentrations when the ferromagnetic phase of the alloy is well developed—that is not very close to the onset concentration. The validity of this assumption is supported by many theoretical investigations on the fcc phase of Fe for which a high-spin state, stable at high atomic volume and favoring the strong ferromagnetism—that is, an almost full spin-up band—is expected. Therefore, the observed decrease of the magnetic moment by $\sim 0.95\mu_B$ per additional $(3d+4s)$ electron, which is made available by the addition of Cu, could be explained by a charge transfer mechanism in which a transfer of electrons takes place from the delocalized $(s+p)$-like bands to the spin-down $3d$-like band of Fe. Although rather schematic, such a model has the advantage of giving quite a simple account of the linear trend of the bulk magnetization. Under the simplifying hypothesis that the electronic charge is transferred at a constant rate, the magnetic moment of Fe in the alloy, $\mu_{\rm Fe}$, can be written as

$$\mu_{\rm Fe}=\frac{\mu}{x_{\rm Fe}}=\mu^0_{\rm Fe}-\frac{1-x_{\rm Fe}}{x_{\rm Fe}}n_{\rm ct}, \tag{1}$$

where μ is the bulk magnetic moment of the alloy, $\mu^0_{\rm Fe}$ is the magnetic moment of Fe with no charge transfer occurring, $x_{\rm Fe}$ is the Fe concentration, and $n_{\rm ct}$ is the number of electrons per added Cu atom that are transferred to the spin-down band of Fe. Equation (1) accounts also for the onset concentration for ferromagnetism, which, in this model, turns out to be directly related to the amount of charge transfer occurring in the system. Assuming the onset concentration at 5% Fe and taking $d\mu/dx_{\rm Fe}=2.85$, one finds $\mu^0_{\rm Fe}=2.707\mu_B$ and $n_{\rm ct}=0.143$, which are quite reasonable values. It is important to observe that, because of the finite value of the onset concentration $n_{\rm ct}$ *must* be positive; that is, electronic charge is transferred towards the spin-down band of Fe. Although this

model is rather appealing in its simplicity, the weakest assumption is that of a concentration-independent charge transfer.

As to the behavior of the bulk magnetization curve at Fe concentration higher than 30%, a mechanism different from the simple charge transfer should be invoked to account for the observed nonlinear trend. The analysis of the neutron diffraction data, for which the bulk magnetization data represent a constraint to be fullfilled, can help in clarifying those aspects.

The magnetic structure factors $F_M(\mathbf{G})$ measured in the neutron diffraction experiment are the series coefficients of the expansion of the spin density, $s(\mathbf{r})$, in the Fourier lattice series, that is

$$F_M(\mathbf{G}) = \int_{\Omega_0} d\mathbf{r}\, s(\mathbf{r}) e^{-i\mathbf{G}\cdot\mathbf{r}},$$

Ω_0 being the unit cell volume, and they are commonly written in terms of the bulk magnetic moment μ and the magnetic form factor $f(\mathbf{G})$ of the alloy. In the present system, because of the topological disorder and using a primitive unit cell, the following relationship holds:

$$F_M(\mathbf{G}) = \mu f(\mathbf{G}), \tag{2}$$

which amounts to a definition of the experimental magnetic form factors $f(\mathbf{G})$ over the reciprocal lattice vectors $\mathbf{G}$. Equation (2) can, alternatively, be exploited to deduce the magnetic moment using, however, a model representation for the magnetic form factor. Assuming Cu to give a negligible contribution to the magnetic properties, this approach consists in fitting the experimental magnetic structure factors $F_M(\mathbf{G})$ by means of an appropriate magnetic form factor of Fe with the magnetic moment left as a free parameter. Clearly, the magnetic moments resulting from this procedure must be comparable, within the experimental uncertainties, with the bulk magnetization data. Sound discrepancies among the two sets of data could only result from a not adequate model form factor or not reliable experimental $F_M(\mathbf{G})$ data.

To ascertain this point, we first carried out the fitting procedure whose crucial point is the choice of the model form factor. Indeed, a form factor representative of Fe in an fcc matrix must be used and, in the simplest picture, it can be taken as independent of the alloy composition. As a form factor appropriate to fcc Fe in the metallic phase, we chose that of Fe in the ordered compound $FeNi_3$, the spin density of which was measured by Cable and Wollan.[10] Indeed, in an ordered phase the magnetic moments and the spherical form factors of both the components of the alloy can be unambiguously deduced from the experimental structure factors. From the $FeNi_3$ data[10] we obtained magnetic moments and spherical form factors of both Fe and Ni using the standard data analysis procedure described in Ref. 27 and accounting for the noncomplete degree of order of the sample. The form factor of Fe, as obtained from $FeNi_3$, was strikingly coincident with that of the free ion Fe^{2+} as quoted in Ref. 28. Both form factors are shown in Fig. 4. Using this form factor for fcc Fe, we carried out the fit to the experimental structure factors $F_M(\mathbf{G})$ and we obtained the magnetic moments $\mu_{\rm fit}$, which are shown in Fig. 3 in comparison with the bulk magnetization data. The two sets of data have the same trend, although the absolute values are different for the two alloys at 50 and 60 at. % concentration.

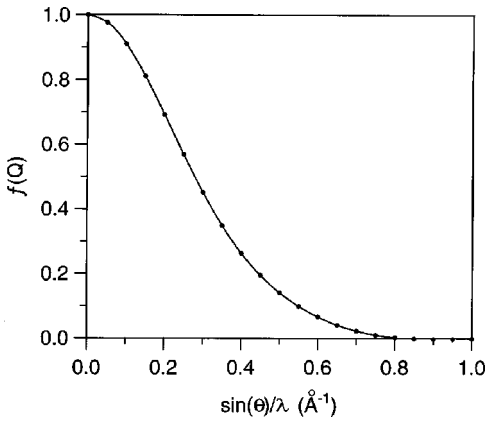

FIG. 4. Form factors of fcc Fe vs sin $(\vartheta)/\lambda$. Dots: form factor of the iron atom in the ordered compound $FeNi_3$ as deduced from the experimental data of Ref. 10. Solid line: form factor of the free ion Fe^{+2} (Ref. 28).

The possibility that the differences shown in Fig. 3 were due to unreliable experimental structure factors was considered carefully. In particular, the effect of the beam depolarization, which directly affects the flipping ratio and hence the structure factors, was further checked. It was found that possible inaccuracies in the structure factors originating from depolarization effects not properly taken into account were to rule out. Indeed, the agreement between the two sets of magnetic moment data, μ and $\mu_{\rm fit}$, for the 50 and 60 at. % alloys would be possible only with unphysical values of the flipping ratio of the Fe_8Co_{92} crystal. Considering that 34 is the expected value of the Fe_8Co_{92} flipping ratio for operation of the spectrometer in ideal conditions, a value of 37 would be necessary to bring the neutron data upon the bulk magnetization data in the case of the $Fe_{50}Cu_{50}$ sample and against the measured value of 15. In the case of $Fe_{60}Cu_{40}$, the Fe_8Co_{92} flipping ratio should take a value of 19 against the measured value of 8.

The reliability of the structure factor data being assessed, the difference observed in Fig. 3 can be ascribed only to a poor representation of the Fe-Cu system by means of the chosen form factor or to a concentration dependence of the form factor itself. A guess on the concentration dependence of the form factor can come from the experimental form factors, as obtained from Eq. (2) where the bulk magnetic moment has to be used. The experimental form factors are shown in Fig. 5. Although the data exhibit rather sizeable error bars, a trend versus concentration of the experimental form factors can be identified. This behavior was quantified by calculating the following χ^2 ratio

$$\frac{\chi^2_{\rm expt}}{\chi^2_{\rm fit}} = \frac{\Sigma_{\mathbf{G}}[F_M(\mathbf{G}) - \mu f_{\rm mod}(G)]^2/\sigma^2(G)}{\Sigma_{\mathbf{G}}[F_M(G) - \mu_{\rm fit} f_{\rm mod}(G)]^2/\sigma^2(G)}, \tag{3}$$

where $\sigma^2(G)$ is the standard deviation of $F_M(\mathbf{G})$, $f_{\rm mod}(G)$ is the model form factor of fcc Fe from either the $FeNi_3$ data or the Fe^{2+} free ion (see Fig. 5), and μ and $\mu_{\rm fit}$ are, as before, the bulk and fitted magnetic moments. This ratio takes the values 1.0, 1.3, 2.0, and 2.6 on increasing the Fe concentra-

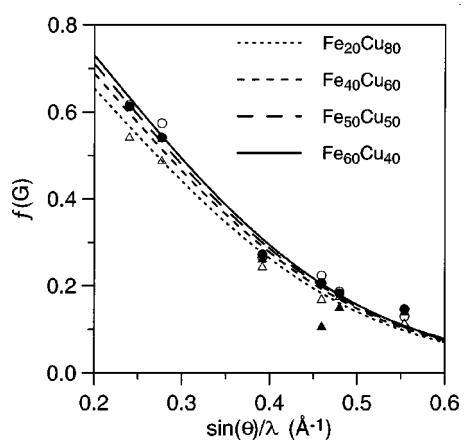

FIG. 5. Experimental form factors $f(\mathbf{G})$ vs $\sin(\vartheta)/\lambda$ for the four alloys. $Fe_{20}Cu_{80}$: open triangles. $Fe_{40}Cu_{60}$: solid triangles. $Fe_{50}Cu_{50}$: circles. $Fe_{60}Cu_{40}$: dots. The curves are smooth lines through the data points as guides to the eye.

tion for the four alloys we studied. This result indicates that the form factor $f_{\mathrm{mod}}(G)$ is an adequate representation for the two alloys with 20 and 40 at. % Fe, whereas the form factor of the two high-Fe-concentration alloys, namely, 50 and 60 at. %, differs appreciably from $f_{\mathrm{mod}}(G)$. The experimental structure factors $F_M(\mathbf{G})$ for the $Fe_{60}Cu_{40}$ sample are shown in Fig. 6 where $\mu f_{\mathrm{mod}}(G)$ and $\mu_{\mathrm{fit}} f_{\mathrm{mod}}(G)$ are also shown as continuous functions of $\sin(\theta)/\lambda$.

From the above analysis we conclude that only the low-iron -concentration alloys can be satisfactorily described by the Fe form factor as observed in $FeNi_3$. Therefore, a possible approach to the description of the magnetic properties of the Fe-Cu system could be to model the structure factors by means of composition-dependent magnetic moments and form factors. This approach is, however, so unrestricted as to prevent recognition of the responsible physical mechanisms. Alternatively, the magnetic structure factors can be modeled by assuming the coexistence of more than one magnetic state for the iron atoms in the alloy, each state associated with a magnetic moment and a form factor. This approach assumes that the local environment affects the magnetic state of Fe, so that the composition dependence of the magnetic structure

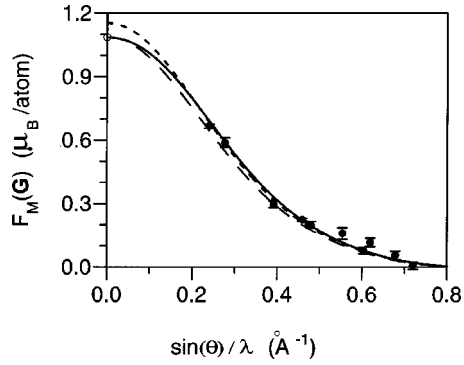

FIG. 6. Magnetic structure factor of $Fe_{60}Cu_{40}$ at 5 K. Dots: experimental data. Dashed line: $\mu_{\mathrm{fit}} f_{\mathrm{mod}}(G)$. Long-dashed line: $\mu f_{\mathrm{mod}}(G)$. $f_{\mathrm{mod}}(G)$ is the model form factor of fcc Fe shown in Fig. 4. Solid line: curve calculated according to the model of Eqs. (4), (5), and (6) (see text). The circle at $\sin(\vartheta)/\lambda = 0$ is the bulk magnetization data.

factors arises from the composition dependence of the possible local environments. The simplest model would then assume the presence of only two possible magnetic states for Fe, which are connected to the local environment of each atom. Of course, such a local environment model attributes the change of the alloy structure factors to a well-defined mechanism, i.e., the direct magnetic interaction between two Fe atoms at nearest-neighbor sites.

We preferred to analyze the magnetic structure factor data by following this second approach and for two main reasons: (a) at high iron concentration the nonlinear trend of the magnetization looks very similar to that observed in both Ni-Mn (Refs. 27 and 29) and Fe-Ni (Ref. 30) ferromagnetic alloys. In Mn-based alloys, the nonlinear dependence of the magnetization versus composition is ascribed to local environment effects induced by the strong antiferromagnetic coupling between neighboring Mn atoms. (b) This approach is strongly supported by the existing theoretical literature on the fcc phase of metallic iron. Indeed, the results of the theoretical investigations point out the stability of only two magnetic states of fcc Fe: the first state, called the low-spin state, is associated with a magnetic moment of $\sim 1\mu_B$, it is stable at low atomic volume, and it favors the antiferromagnetic coupling; the second, the high-spin state, is stable at high atomic volume, it is associated with a magnetic moment ranging from $2.5\mu_B$ to $3\mu_B$, and it favors the strong ferromagnetism. Therefore, coherently with the conjectured double magnetic state of Fe the measured structure factors were written as a weighted sum of two contributions, that is

$$F_M(\mathbf{G}) = [x_1\mu_1 f_1(\mathbf{G}) + x_2\mu_2 f_2(\mathbf{G})]x_{\mathrm{Fe}}, \tag{4}$$

where μ_1 and μ_2 are the magnetic moments of the iron atoms in the two magnetic states, x_1 and $x_2 = 1 - x_1$, and $f_1(\mathbf{G})$ and $f_2(\mathbf{G})$ the corresponding fractions and form factors. The bulk magnetic moment was also written as a weighted sum:

$$\mu = [x_1\mu_1 + x_2\mu_2]X_{\mathrm{Fe}}. \tag{5}$$

The fit to the measured structure factors and bulk magnetization data through Eqs. (4) and (5) was carried out under the following assumptions: (a) the magnetic form factors (f_1 and f_2) and the magnetic moments (μ_1 and μ_2) were almost independent of the alloy composition; (b) the magnetic moment μ_1 was deduced from Eq. (1); (c) the magnetic moment μ_2 was left as a free parameter; (d) the form factor f_1 was that deduced for the iron atom in the $FeNi_3$ intermetallic compound which was assumed to be representative of Fe in an fcc matrix; (e) the form factor f_2 was modeled by that appropriate to a hydrogenic atom with angular momentum equal to 2, that is,

$$f_2(Q) = \frac{\lambda^8(3\lambda^4 - 10Q^2\lambda^2 + 3Q^4)}{3(\lambda^2 + Q^2)^6}, \tag{6}$$

with λ left as a free parameter.

The fit was carried out by varying λ and μ_2 over a quite broad range with x_1, and hence $x_2 = 1 - x_1$, fixed in order to get the correct bulk magnetization. The fit was performed including all the experimental structure factors of all the four alloys at the same time. In this way we got the best estimate of μ_2 and $f_2(Q)$ at all the iron concentrations. It turned out

that the χ^2 surfaces of the fit had a rather well-defined minimum around $\mu_2=(-0.56\pm0.10)\mu_B$ and $\lambda/4\pi=0.35\pm0.10\,\text{Å}^{-1}$. Such a minimum indicates that a second magnetic state with a negative magnetic moment and a rather broad distribution of the magnetization through the unit cell is favored with the present experimental data. As expected, the concentration of the negative magnetic moment state of Fe increases on increasing the iron concentration, and it takes the values $x_2=0.021\pm0.025$ at 20 at.% Fe, $x_2=0.064\pm0.015$ at 40 at.% Fe, $x_2=0.146\pm0.010$ at 50 at.% Fe, and $x_2=0.253\pm0.010$ at 60 at.% Fe. The magnetic structure factor resulting from the present fit is shown as a solid line in Fig. 6 in the case of the $Fe_{60}Cu_{40}$ alloy. Unfortunately, the quality of the present data does not allow for a more quantitative analysis of the shape of the spin density of the second magnetic state of Fe and we had to rely on the model function of Eq. (6). Nonetheless, conjecturing the second magnetic state provides a model within which both the experimental neutron data and the bulk magnetization data find a simple and common interpretation.

We want to note that the present data could have been described also by an almost constant negative magnetic moment density plus a magnetic moment density well represented by the form factor of the free Fe^{2+} ion. In such a model the negative magnetic moment is expected to originate from the polarization of those electrons with the most diffuse distribution throughout the unit cell, and hence it is expected to be proportional to the bulk magnetic moment. This model would therefore predict a linear trend of the magnetization as a function of the composition.

Further support of the present description of this system comes also from the recent paper of Xu *et al.*[31] The authors report the presence of two different components, with a different distribution of hyperfine fields, in the Mössbauer spectra measured in $Fe_{50}Cu_{50}$ samples. Such a behavior is possibly ascribed to variations in the magnetic moment of the Fe atoms depending on the local environment.

IV. CONCLUSIONS

Polarized neutron diffraction measurements on four samples of metastable fcc Fe-Cu alloys were performed. These measurements, together with bulk magnetization data, allowed for a description of the magnetic state of iron within the fcc environment. First of all, the neutron diffraction data confirm the bulk magnetization and Curie temperature results which show that the system is nonmagnetic for concentrations below ~5 at.% Fe. Above this concentration the magnetic moment increases at a rate of about $2.85\mu_B$/Fe atom with a pronounced tendency to level off at higher Fe concentration, similar to what is observed in the case of Fe-Ni.[30] From these results one deduces that Fe-Cu represents a new *fcc* system on the right-hand side of the Slater-Pauling curve, other than the classical Ni-Cu alloys,[15–18] where one observes the onset of the ferromagnetism at a finite concentration of the magnetic component. The onset and linear dependence of the bulk magnetization on the Fe concentration for $x_{Fe}\leqslant0.3$ were interpreted by means of the simple model described in Sec. III and related to the occurrence of charge transfer from Cu to Fe bands.

The nonlinear trend of the bulk magnetization as the concentration of Fe is increased over 30%, which is very similar to that observed in Mn-Ni and Fe-Ni alloys, was interpreted on the basis of the two-magnetic-state model of Fe, using different form factors and different magnetic moments for the two states of Fe. From the analysis of the present diffraction data, together with the bulk magnetization data, it was found that a good fit is obtained only if the magnetic moment of the additional magnetic state of Fe is negatively aligned with respect to the ferromagnetic matrix. The results of the fit strongly support the idea that the occurrence of the negative magnetic moment state is related to the local environment of each Fe atom. If this is the case, any theoretical calculation performed in systems like the present one should not neglect these local effects. The presence of a second magnetic state of Fe gets further support from the recent results of Mössbauer measurements[31] in $Fe_{50}Cu_{50}$, where the presence of two magnetic states for iron is suggested to explain the observed spectra. Indeed, a value of the concentration x_2 similar to that found in Ref. 31 is recovered by the present analysis at the best fit value of μ_2. The interpretation of the data in terms of the two-state model is also supported by the results of Ref. 24 where the magnetization changes after annealing were discussed.

We note that alternative models can be proposed to explain nonlinear trends of the bulk magnetization, involving, for instance, changes of the band splitting of the electron density of states with concentration. However, in the case of Fe-Cu a variation of the band splitting with concentration does not account for the nonlinear trend of the bulk magnetization. Indeed, since the band splitting is expected to *increase* with *increasing* the iron content, this would result in an *increase* of the Fe magnetic moment on *increasing* the iron concentration. This behavior would be just the reverse of what observed—that is, a *decrease* of the Fe magnetic moment at *high* iron content.

Finally, we observe that further investigation by means of polarized diffuse neutron scattering measurements would be valuable. Such an investigation would allow for a quantitative determination of the individual average magnetic moments as well as of their fluctuations. Moreover, the analysis of the nuclear contribution to the diffuse scattering would give information on the atomic short-range order. This is of great importance to define the effect of the local environment on the magnetic moment.

ACKNOWLEDGMENTS

The Institut Laue-Langevin is acknowledged for having provided the neutron beam time. We wish to thank E. Lelievre-Berna for technical assistance during the measurements and for helpful discussions. We are very grateful to Dr. D. Fiorani for performing bulk magnetization measurements on our samples. We are indebted to P. J. Brown for help during the data collection and for her stimulating criticism when reading this manuscript.

APPENDIX

The data reduction procedure, although of rather standard type as to its main steps, has requested the development of appropriate codes to handle the depolarization effects, the

spin-dependent background transmission, and the spin-dependent sample attenuation. Moreover, because of the rather low resolution, possible superpositions of the tails of adjacent Bragg peaks had to be carefully treated in order to obtain the correct intensity to be integrated over each Bragg peak.

First of all, the background was subtracted by means of the following relationship:

$$I_s = I_m - I_{\text{back}} = I_m - [T_B I_0 + (1 - T_B) I_{\text{abs}}], \qquad \text{(A1)}$$

where I_m is the measured sample intensity and I_{back} is the background intensity with I_0 the intensity measured with the empty cell, I_{abs} the intensity measured from the cell filled with B_4C powder, and T_B the forward sample transmission. All the intensities and transmission in Eq. (A1) are dependent on the spin state of the incoming neutrons. T_B was calculated accounting for both the true absorption and the attenuation due to the spin-dependent scattering, the spin-dependent linear attenuation coefficient of the sample being

$$\mu = n(\sigma_c + \sigma_i + \sigma_a),$$

where n is the sample number density, and σ_i and σ_a are the incoherent scattering and the absorption cross sections per atom. σ_c is the coherent scattering cross section per atom due to Bragg processes taking place inside the sample, which, accounting for the spin-dependent magnetic cross section, is given by

$$\sigma_c = \frac{N_c}{2\lambda^2} \sum_{d(G) \geqslant \lambda/2} F^2(\mathbf{G}) d(\mathbf{G}), \qquad \text{(A2)}$$

where

$$F^2(\mathbf{G}) = b^2 + q^2 p(\mathbf{G})^2 \pm 2 q^2 b p(\mathbf{G}).$$

In Eq. (A2), $d(\mathbf{G})$ is the d spacing of the reflecting planes corresponding to the reciprocal lattice vector $\mathbf{G}$, b and $p(\mathbf{G})$ are the nuclear and magnetic scattering lengths, and $q^2 = (1 + \sin^2 \varphi)/2$, φ being the Bragg angle. As apparent from these equations, the attenuation correction requires an approximate estimate of the magnetic structure factor of the sample. The form factor[28] of the free ion Fe^{2+} and a fixed magnetic moment of $2.2\mu_B$ per iron atom were employed as a first guess of the magnetic structure factor of the alloy. This approximation is not crucial, since the magnetic contribution to the total cross section is fairly small and never exceeds 10%. The transmission T_B was then determined by numerical integration over the sample volume using the so-deduced linear attenuation coefficient μ.

The intensity corrected for background was fitted to the diffraction pattern appropriate for an fcc sample, leaving the lattice parameter, the peak intensity of each reflection, and the residual background, due to both incoherent and diffuse scattering and modeled by a second degree polynomial, as free parameters. The width of the Bragg peaks was described by the approximate two-parameters formula

$$W = W_0 + D_0 \tan(\vartheta_B - \vartheta_B^{\text{mon}}),$$

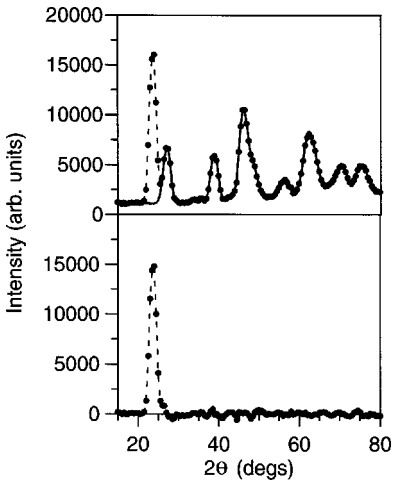

FIG. 7. Typical result of the fitting procedure (see the Appendix) on the background-free spin-up data of $Fe_{60}Cu_{40}$ at 5 K (dots). Upper panel: the solid line is the fitted curve. Lower panel: first peak data after subtraction of the fitted curve. Dashed lines are a guide to the eye.

where ϑ_B^{mom} is the monochromator Bragg angle and W_0 and D_0 were also left as free parameters. Use of this approximate equation is reasonable since the sample scattering angle was always greater than the monochromator Bragg angle. The quality of the fit was found to be quite good in all cases and even in those regions where different reflections strongly ovelap because of the rather poor resolution. The main reason for developing such a fitting procedure was the need of obtaining clean peaks—that is, free from residual background and possible contributions from adjacent peaks—for each Bragg reflection from which the integrated intensities could be deduced. Therefore, the fitted curve was employed to subtract the tails of all the reflections but that to be analyzed from the experimental data. In other words, use of the fitting procedure was limited to the subtraction of the contribution arising from neighboring reflections on the tails of a given peak, and the integrated intensity of each reflection was deduced by direct integration of the isolated experimental peak. This procedure is expected to reduce the effect of the tails providing a reliable integrated intensity for those reflections which are very close to each other without resorting too much to the results of the fit. A typical result of this procedure is shown in Fig. 7.

Depolarization effects brought about by the sample were treated by seeking a solution of the appropriate neutron transport equations. With a finite transition probability between the two neutron spin states, the transport equations can be written as

$$dN_\uparrow = (-wN_\uparrow + wN_\downarrow - \mu_\uparrow N_\uparrow) d\tau,$$

$$dN_\downarrow = (-wN_\uparrow + wN_\downarrow - \mu_\downarrow N_\downarrow) d\tau,$$

where $dN_\uparrow (dN_\downarrow)$ represents the variation of the spin-up (-down) neutron flux when the neutron path inside the sample is $d\tau$, w is the spin reversal probability due to the

sample depolarization, and $\mu_\uparrow(\mu_\downarrow)$ is the spin-dependent linear attenuation coefficient. By analytic integration of these equations along the path from the container wall to the point where a scattering event takes place, under the assumption of a uniform sample, $N_\uparrow(\tau)$ and $N_\downarrow(\tau)$ were obtained for any given value of the incoming neutron flux and the incoming beam polarization. The explicit formulas of $N_\uparrow(\tau)$ and $N_\downarrow(\tau)$ are

$$N(\tau)=N_\uparrow(\tau)+N_\downarrow(\tau)=B\exp(-\mu_1\tau)+C\exp(-\mu_2\tau),$$

$$\begin{aligned} n(\tau)=N_\uparrow(\tau)-N_\downarrow(\tau)=&\frac{2}{\mu_\uparrow-\mu_\downarrow}\\ &\times\left[w+\sqrt{\left(\frac{\mu_\uparrow-\mu_\downarrow}{2}\right)^2+w^2}\right]B\exp(-\mu_1\tau)\\ &+\frac{2}{\mu_\uparrow-\mu_\downarrow}\\ &\times\left[w-\sqrt{\left(\frac{\mu_\uparrow-\mu_\downarrow}{2}\right)^2+w^2}\right]C\exp(-\mu_2\tau), \end{aligned}$$

where

$$\begin{aligned} B=&\left(1-\frac{1}{2\sqrt{1+\left(\frac{\mu_\uparrow-\mu_\downarrow}{2w}\right)^2}}\right)N_0\\ &+\frac{1}{2\sqrt{1+\left(\frac{2w}{\mu_\uparrow-\mu_\downarrow}\right)^2}}n_0, \end{aligned}$$

$$\begin{aligned} C=&\left(1+\frac{1}{2\sqrt{1+\left(\frac{\mu_\uparrow-\mu_\downarrow}{2w}\right)^2}}\right)N_0\\ &-\frac{1}{2\sqrt{1+\left(\frac{2w}{\mu_\uparrow-\mu_\downarrow}\right)^2}}n_0, \end{aligned}$$

$$\mu_{1/2}=\frac{\mu_\uparrow+\mu_\downarrow}{2}+w\pm\sqrt{\left(\frac{\mu_\uparrow-\mu_\downarrow}{2}\right)^2+w^2},$$

$n(\tau=0)$ being the incident beam polarization and $N(\tau=0)$ being the incoming neutron flux.

Applying this approach to the analysis of the flipping ratio measurements of the (200) reflection from the $Co_{92}Fe_8$ crystal mounted inside the Fe-Cu powder samples, it was possible to deduce the experimental values of the transition probability w. Indeed, the relevant path in this case is only that from the container wall to the $Co_{92}Fe_8$ crystal, and the relationships for $N_\uparrow(\tau)$ and $N_\downarrow(\tau)$ were numerically averaged over all the possible paths of this kind. The w values deduced from the depolarization measurements are reported in Table I. Finally, the experimental flipping ratios of the Fe-Cu samples were corrected for depolarization effects, making use of the so-deduced w values and performing the numerical average of $N_\uparrow(\tau)$ and $N_\downarrow(\tau)$ over all possible paths from the container wall to the point where the scattering event takes place—namely, everywhere inside the sample volume. It is worth to note that a simultaneous correction for depolarization and spin-dependent attenuation is obtained as a result of this procedure.

[1] W. Kohn and L. J. Sham, Phys. Rev. A **140**, A1133 (1965).
[2] G. E. W. Bauer, Phys. Rev. B **27**, 5912 (1983).
[3] H. J. F. Jansen, K. B. Hathaway, and A. J. Freeman, Phys. Rev. B **30**, 6177 (1984).
[4] C. Amador, W. R. L. Lambrecht, and B. Segall, Phys. Rev. B **46**, 1870 (1992).
[5] V. L. Moruzzi, P. M. Marcus, and J. Kubler, Phys. Rev. B **39**, 6957 (1989).
[6] Y. Tsunoda, J. Phys.: Condens. Matter **1**, 10 427 (1989).
[7] Y. Endoh and Y. Ishikawa, J. Phys. Soc. Jpn. **30**, 1614 (1971).
[8] P. Bisanti, G. Mazzone, and F. Sacchetti, J. Phys. F: Met. Phys. **17**, 1425 (1987).
[9] F. Menzinger and A. Paoletti, Nuovo Cimento Soc. Ital. Fis., B **10**, 565 (1972).
[10] J. W. Cable and E. O. Wollan, Phys. Rev. B **7**, 2005 (1973).
[11] F. Menzinger, F. Sacchetti, and F. Leoni, Nuovo Cimento Soc. Ital. Fis., B **20**, 1 (1974).
[12] F. Dupre', F. Menzinger, and F. Sacchetti, J. Phys. F: Met. Phys. **11**, 2179 (1981).
[13] Y. Ito, J. Akimitsu, M. Matsui, and S. Chikazumi, J. Magn. Magn. Mater. **10**, 194 (1979).
[14] O. N. Mryasov, V. A. Gubanov, and A. I. Liechtenstein, Phys. Rev. B **45**, 12 330 (1992).
[15] F. Sacchetti, P. De Gasperis, and F. Menzinger, Phys. Status Solidi B **76**, 309 (1976).
[16] R. A. Medina and J. W. Cable, Phys. Rev. B **15**, 1539 (1977).
[17] J. W. Cable, Phys. Rev. B **36**, 8837 (1987).
[18] T. J. Hicks, J. Phys. F: Met. Phys. **7**, 481 (1977).
[19] J. Eckert, J. C. Holzer, C. E. Krill III, and W. L. Johnson, J. Appl. Phys. **73**, 2794 (1993).
[20] E. Ma, M. Atzmon, and F. E. Pinkerton, J. Appl. Phys. **74**, 955 (1993).
[21] P. Crespo, A. Hernando, R. Yavari, O. Drbohlav, A. Garcia Escorial, J. M. Barandiaran, and I. Orue, Phys. Rev. B **48**, 7134 (1993).
[22] P. Crespo, A. Hernando, and A. Garcia Escorial, Phys. Rev. B **49**, 13 227 (1994).
[23] V. G. Harris, K. M. Kemner, B. N. Das, N. C. Koon, A. E. Ehrlich, J. P. Kirkland, J. C. Woicik, P. Crespo, A. Hernando, and A. Garcia Escorial, Phys. Rev. B **54**, 6929 (1996).
[24] G. Mazzone and M. Vittori Antisari, Phys. Rev. B **64**, 441 (1996).
[25] K. Sumiyama and Y. Nakamura, in *Rapidly Quenched Metals*, edited by S. Steeb and H. Warlimont (Elsevier, Amsterdam, 1985), p. 859.
[26] C. L. Chien, S. H. Liou, D. Kofalt, W. Yu, T. Egami, and T. R.

McGuire, Phys. Rev. B **33**, 3247 (1986).
[27] G. Mazzone, C. Petrillo, F. Sacchetti, and M. Scafi, Phys. Rev. B **46**, 11 665 (1992).
[28] *International Tables for X-ray Crystallography*, edited by J. A. Ibers and W. C. Hamilton (Kluwer Academic, Dordrecht, 1989), Vol. IV.
[29] A. Paciaroni, C. Petrillo, and F. Sacchetti, Solid State Commun. **103**, 97 (1997).
[30] J. Crangle and G. C. Hallam, Proc. R. Soc. London, Ser. A **272**, 119 (1963).
[31] J. Xu, G. S. Collins, L. S. J. Peng, and M. Atzmon, Acta Mater. **47**, 1241 (1999).